Available online at www.sciencedirect.com
ScienceDirect
Journal of the European Ceramic Society 31 (2011) 2031–2036
www.elsevier.com/locate/jeurceramsoc

Ball-on-ring test in ceramic materials revisited by means of fluorescence piezospectroscopy

Alessandro Alan Porporati [a], Takahiro Miyatake [b], Kristina Schilcher [c], Wenliang Zhu [a], Giuseppe Pezzotti [a,*]

[a] *Kyoto Institute of Technology, Ceramic Physics Laboratory, Sakyo-ku, Matsugasaki, Kyoto 606-8585 Japan*
[b] *Panasonic Electric Works Co., Ltd., Micro Fabrication Process Development Department, Kadoma, Osaka 571-8686 Japan*
[c] *CeramTec AG, Development Department, Plochingen 73207 Germany*

Received 20 October 2010; received in revised form 27 April 2011; accepted 7 May 2011
Available online 1 June 2011

Abstract

Ball-on-ring test is widely used to measure the biaxial strength of brittle materials by often making the approximation that the pressure applied by the ball in the central loading region is uniform. The purpose of the present study is to demonstrate the limits of such approximation by means of piezospectroscopy and to substantiate the spectroscopic findings with calculations based on finite element modeling (FEM). In addition, we shall discuss in some detail the validity of theoretical expressions previously developed by Kirstein and Woolley for radial and tangential bending stresses in the case of a uniformly distributed concentric load applied at the center of the disk loading region. A comparison is also offered between the experimentally retrieved radius of such region and those computed by theoretical models. Errors in estimating the radius of the central loading region, which have led in the past to controversial discussions, have been shown to play a minor role in the analysis of the overall stress field.

Keywords: Ball on ring; Alumina; Piezospectroscopy; Stress; FEM

1. Introduction

Uniaxial bending is the loading configuration of the most commonly performed tests for evaluating the strength of ceramic materials. Besides their easier approach, however, bending geometries might not appropriately re-create the multiaxial loading conditions occurring in real service applications. In alternative, the ball-on-ring test can be performed on thin disks to measure the biaxial strength of brittle materials.[1–9] However, the stress distribution involved with a biaxial loading apparatus on a brittle thin disk has not been yet fully elucidated in its complete profile, mainly because of a lack of spatial resolution for the available *in situ* stress measurement techniques (e.g., adopting strain gauge or X-ray diffraction methods).

In the last decade, piezospectroscopy (PS) has been widely used to measure local stress distributions both in single-crystalline and polycrystalline materials.[9–12] The PS method relies on the perturbation of vibrational (or energy) bands due to a stress field.[10] Such perturbation effect can be, for example, evaluated by monitoring the stress-induced shift of selected Raman or fluorescence peaks. The PS technique has also been commonly used to extract stress magnitudes in polycrystalline alumina materials, since the R1 (14,400 cm^{-1}) and R2 (14,430 cm^{-1}) lines of the alumina fluorescence spectrum, which are emitted from chromium (Cr^{3+}) impurity sites, have shown reliable dependence on applied stress.[9–12] A comprehensive description of the phenomenon was first given by Ma and Clarke[9] and later by other authors.[11,12]

In this paper, we shall revisit the mechanics of the ball-on-ring test and attempt to locate the most precise computational procedure for analyzing the related surface stress field, thus providing a tool for accurate strength analysis in ceramic polycrystals subjected to a biaxial stress field. The main purpose here is to judge about the validity of already existing models, with emphasis placed on explicitly describing the stress field in the central area ($0 < r < b$ with b radius of the loading region) of the loaded plate, which has not been unfolded yet. For doing so, we directly measured the stress distribution by means of the PS tool, which is

* Corresponding author.
E-mail address: pezzotti@kit.ac.jp (G. Pezzotti).

0955-2219/$ – see front matter © 2011 Elsevier Ltd. All rights reserved.
doi:10.1016/j.jeurceramsoc.2011.05.009

shown possessing sufficient spatial resolution to conspicuously reduce smoothing effects due to the finite size of the measurement probe. In this latter context, the effect of a finite probe size is directly evaluated and deconvoluted from fluorescence spectral analysis. We shall finally give an experimental estimate of the dimensions of the loading area at the center of the sample and compare it with values obtained from current theories.

2. Theoretical background

In a finely grained and untextured polycrystal, the PS effect can be expressed by the following formula:

$$\Delta\nu = \Pi\sigma_h \tag{1}$$

where $\Delta\nu$ is the difference between the peak wavenumber at the stressed location and the peak wavenumber of a reference stress-free state (i.e. the unloaded disk in our case), Π is the PS coefficient (i.e., equal to 7.61 cm^{-1}/GPa for the R2 line in polycrystalline alumina[9]) and σ_h represents the hydrostatic stress. In the case of the biaxial stress state generated by a ball-on-ring loading apparatus can be defined as:

$$\sigma_h = \frac{\sigma_r + \sigma_t}{3} \tag{2}$$

Of interest here is that, by using an optical microprobe, Eq. (1) provides a means to measure the stress distribution inside the loading region, as developed along any radial direction on the surface of an alumina disk subjected to ball-on-ring test.

In the ball-on-ring test, a disk-shaped sample is supported by a ring and loaded centrally by a ball (Fig. 1). Axisymmetric loading of the disk in this arrangement produces radial and tangential stresses on the ball-side face of the specimen. Kirstein and Woolley[1] have given an analytical solution for both radial and tangential stresses as a function of the number of supporting points and of their angular position for $0 < r < b$. In the case of a ball-on-ring apparatus, a large m number of supporting points can be treated as a continuous supporting line, and the equations written as follows:

$$\sigma_r = \frac{EM_r t}{2D} \tag{3}$$

$$\sigma_t = \frac{EM_t t}{2D} \tag{4}$$

with $D = (Et^3/12)$ for a disk shaped sample, t being the plate thickness and

$$M_r = -\frac{P(1+\nu)(3+\nu)}{8\pi m(\nu-1)}[\psi] + \frac{P(1-\nu)(3+\nu)c^2}{16\pi m(\nu-1)r^2}[\Omega] \tag{5}$$

$$M_t = -\frac{P(1+\nu)(3+\nu)}{8\pi m(\nu-1)}[\psi] - \frac{P(1-\nu)(3+\nu)c^2}{16\pi m(\nu-1)r^2}[\Omega] \tag{6}$$

where

$$\psi = \sum_{s=1}^{m}\left\{\ln\left(1 - 2\frac{ar}{R^2}\cos\varphi_s + \frac{a^2r^2}{R^4}\right) - \frac{(\nu-1)}{(3+\nu)}\left(\frac{r^2}{R^2} - 2\frac{ar}{R^2}\cos\varphi_s + \frac{a^2}{R^2}\right) - \frac{(1-(a^2/R^2))(1-((a^2r^2)/R^4))}{1-2(ar/R^2)\cos\varphi_s + ((a^2r^2)/R^4)}\right\} + \frac{2m(a^2/R^2)}{(1+\nu)} + m - \frac{2m(\nu-1)((b\sqrt{n/n+2})/R)}{(((\nu-1)/(3+\nu))+1)(3+\nu)} + 2m\frac{(\nu-1)}{(3+\nu)}\ln\frac{b}{R} + \frac{2m(\nu-1)}{n(3+\nu)}\left(\frac{(r/R)^n}{(b/R)^n} - 1\right) \tag{7}$$

and

$$\Omega = \sum_{s=1}^{m}\left\{\left(\frac{(\nu-1)^2}{(3+\nu)^2} - 1\right)\ln\left(1 - 2\frac{ar}{R^2}\cos\varphi_s + \frac{a^2r^2}{R^4}\right) + \frac{(1-((a^2r^2)/R^4))^2 - 2(a/R)^2(1-(r^2/R^2))^2}{(1-2(ar/R^2)\cos\varphi_s + ((a^2r^2)/R^4))} - \frac{(1-(r^2/R^2))(1-(a^2/R^2))(1-((a^2r^2)/R^4))^2}{(1-2((ar)/R^2)\cos\varphi_s + ((a^2r^2)/R^4))^2} + \frac{(\nu-1)((r^2/R^2)-(a^2/R^2))^2}{(3+\nu)((r^2/R^2)-2(ar/R^2)\cos\varphi_s + (a^2/R^2))}\right\} + m\left(\frac{(\nu-1)}{(3+\nu)} - 1\right)\left(\frac{r^2}{R^2} - \frac{a^2}{R^2}\right) - \frac{4m(\nu-1)(r/R)^n}{(3+\nu)(n+2)(b/R)^n} \tag{8}$$

with n being an empirical parameter = 2 in the case of a uniformly distributed concentric load, $\varphi_s = \theta - \theta_s = s\cdot(2\pi/m)$, where θ_s is the polar angle subtended by the sth supporting point with $s = 1, 2, 3, \ldots, m$ (cf. Fig. 1).[1] Eqs. (7) and (8) can be greatly simplified by approximating with the case of a concentric (central) load (i.e., letting $b/R = 0$) or to the case of a load uniformly distributed over the entire disk (i.e., letting the ratio $b/R = 1$). It is important to note that the magnitude of maximum stress at the central position of the loading region is always equibiaxial and given by:

$$\sigma_{max} = \left[\frac{3P(1+\nu)}{4\pi t^2}\right]\left\{1 + 2\left[\ln\frac{a}{b}\right] + \left[\frac{(1-\nu)a^2}{(1+\nu)R^2}\right]\left[1 - \frac{b^2}{2a^2}\right]\right\} \tag{9}$$

Unlike Eqs. (3) and (4), the maximum bending stress in Eq. (9) is independent of the number of supporting points. In addition, for a concentric point load, the problem of the stresses in the loading region has been solved by introducing the approximation of a region of constant stress (i.e., as given by Eq. (9)) with finite dimensions (e.g., in Ref. [2]).

For the $r > b$ study case, Vitman and Pukh[7] offered a stress distribution model taking into account the stiffening effect of the

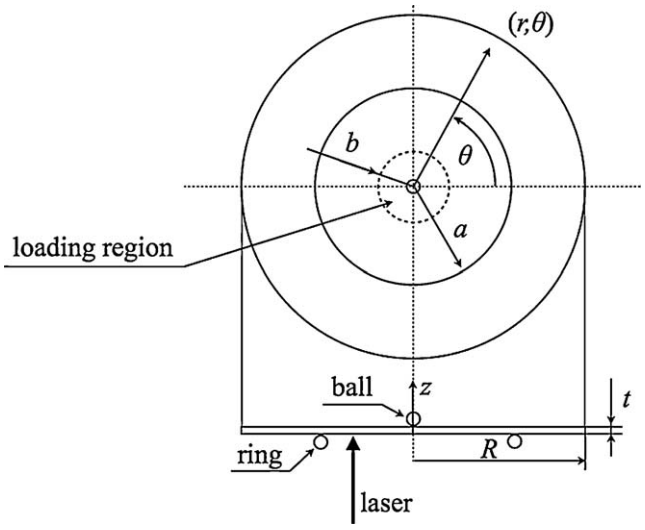

Fig. 1. Schematics of the used ball-on-ring testing configuration showing the geometrical parameters involved with the calculation of radial and tangential stresses.

annular region outside the ring region. The resulting equations are:

$$\sigma_r = \frac{3P(1+\nu)}{4\pi t^2}\left[2\ln\frac{a}{r} + \frac{(1-\nu)}{2(1+\nu)}\left\{\frac{a^2-r^2}{a^2}\right\}\frac{b^2a^2}{r^2R^2}\right] \quad (10)$$

$$\sigma_t = \frac{3P(1+\nu)}{4\pi t^2}\left[2\ln\frac{a}{r} + \frac{(1-\nu)}{2(1+\nu)}\left\{4-\frac{b^2}{r^2}\right\}\frac{a^2}{R^2}\right] \quad (11)$$

where b is the radius of the loading area (i.e., otherwise called constant stress region), R is the radius of the disk and a the radius of the supporting points. Note that as in the maximum stress case, also in the region $r>b$, the stresses are independent of the number of support points. Note that, whatever the selected analytical procedure, in order to calculate stress magnitudes, one needs to retrieve the value of the radius of the loading region, b. The parameter b can be computed according to Westergaard[8]:

$$\begin{aligned} b &= t && \text{for} \quad Z > 1.724t \\ b &= \sqrt{(1.6Z^2+t^2)} - 0.675t && \text{for} \quad Z < 1.724t \\ b &= 0.325t && \text{for} \quad Z \to 0 \end{aligned} \quad (12)$$

where Z is the contact radius of the loading ball, which can be retrieved according to a Hertzian model for the (elastic) contact radius in the case of contact between a plate and a ball[3]:

$$Z = \left(\frac{3P\cdot r_{\text{ball}}}{4E'}\right)^{1/3} \quad \text{with} \quad \frac{1}{E'} = \left[\frac{1-\nu_{\text{disk}}^2}{E_{\text{disk}}}\right] + \left[\frac{1-\nu_{\text{ball}}^2}{E_{\text{ball}}}\right] \quad (13)$$

where P is the load, r_{ball} is the radius of the loading ball, and E_{disk} and E_{ball} are the Young's moduli of disk and ball, respectively.

On the other hand, Shetty et al.[2] determined the radius of the loading region b by using contact stress theory, i.e., assuming $Z \ll t$ and that both ball radius and load are not affecting b significantly. As a result, these researchers obtained an equivalent radius of contact $b \approx t/3$, which can be used in place of b and describes the stresses upon biaxial loading in the ball-on-ring test.

The differences in the interpretation and assignment of b have been the origin for controversies and debates, and the suitability of the available models has been discussed by de With and Wagemans,[3] who confirmed the validity of the Westergaard approximation measuring the bending displacements with strain gauges, while loading a thick glass plate in a ball-on-ring apparatus.

Despite the experimental evidence provided in the paper by de With and Wagemans,[3] in almost all literature papers, the stress distribution caused by the ball-on-ring test in the loading central area ($0<r<b$) is approximately determined by a region of uniform pressure. Actually, the origin of such approximation arises from b being conspicuously smaller than the area probed by strain gauges and, thus, from a lack of knowledge of the actual stress distribution in such a tiny area, which we shall now prove to be not uniform in support to the data by de With and Wagemans.[3] Note that a crude approximation in assuming the stress distribution in the central loading region might lead to a tangible error in understanding the material behavior under the biaxial load and, thus, in assessing the strength of the tested material.

PS experiments using an optical microprobe thus give us a chance to test Kirstein and Woolley's solution for $0<r<b$ (Eqs. (3) and (4)) and Vitman and Pukh's solution for $r>b$ (Eqs. (10) and (11)). Obviously, the former stress distribution is expected to be more sensitive to the parameter b, than the region $r>b$. In order to validate the PS results, we also carry out here a comparison with a stress distribution obtained by a conventional FEM analysis. The geometry of the meshed disk sample is shown in Fig. 2.

3. Experimental procedure

The alumina polycrystalline sample was prepared from a commercially available alumina powder (Almatis GmbH, Germany). After milling, the sample was pressed into disks at 200 MPa, sintered at 1580 °C for 2 h, hot-isostatically pressed (HIPed) under 200 MPa at 1580 °C, and finally post-heat treated at 1580 °C for 2 h. The average grain size of the sintered polycrystal was 1 μm. The samples were then machined into disks $R = 14$ mm and $t = 0.820$ mm in dimension (i.e., according to the geometry shown in Fig. 1) and finely polished (with diamond paste of 1 μm) on both surfaces.

Fluorescence spectra were excited using an argon ion laser operating at 488 nm with an optical power at the sample surface of 6 mW. Such power was low enough to prevent laser-induced heating on the sample surface. The microscope objective was a long working distance 100×, which produced a theoretical spot diameter of 1 μm in the focal plane of the sample. The laser penetration distance (about 30 μm), which has an impact on the stress gradient in depth, can be considered here small in comparison with the disk thickness. This argument will be quantitatively substantiated in a later section with providing a deconvolution procedure on the measured profile of fluorescence shifts. The emitted luminescence was collected and analyzed by

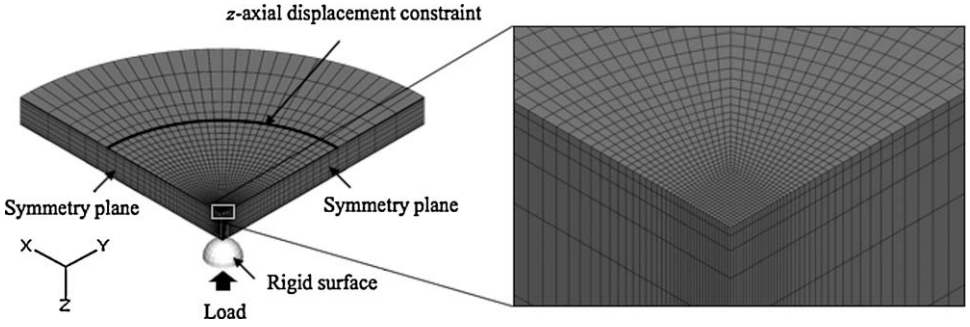

Fig. 2. Meshed geometry and boundary conditions for simulating the ball-on-ring test by FEM and calculating the related stresses in loaded configurations.

a Raman microprobe equipment (T-64000, Horiba-Jobin Yvon, Tokyo, Japan). The chromophoric luminescence doublet emitted from the alumina polycrystal was fitted to two Voigtian curves in order to precisely locate individual band maxima. Spectral fitting procedures were the same as those reported in previous literature.[9–12] By moving the sample under the microprobe by means of an automatized stage (with a step unit of 5 μm), we performed several diametral line-scans from the center of the sample along an arbitrarily selected radial direction. Fluorescence spectra were collected at exactly the same locations with the disk both in the unloaded configuration and under 52, 105.5, 150.1, and 200 N peak loads. Stresses were calculated, according to Eq. (1), by subtracting from the locally recorded spectral position of the chromophoric R2 level peak the position of the same band in the unloaded configuration.

All the equations involved with the present investigation were solved numerically, with the aid of a commercially available computational software package (Mathematica 7.0; Wolfram Research Inc., Champaign, IL).

Calculations involved with the FEM analysis were conducted with the code Abaqus 6.7 (ABAQUS, Dassault Systémes, Woodland Hills, CA).

4. Results and discussion

4.1. Experimentally and theoretically assessed stress field

To judge whether or not available analytical solutions are applicable to the ball-on-ring test, we performed a series of 6 mm radial fluorescence line-scans along the disk diameter as function of applied load. With the PS measurement tool, applied to the fluorescence emission of alumina, only the hydrostatic part of the stress tensor can be assessed. It follows that our experimental data should be compared to the radial and tangential stresses (i.e., as given by Vitman and Pukh for $r > b$ and Kirstein and Wooley for $0 < r < b$) after extracting the hydrostatic component of the stress tensor from these models. b was experimentally measured by fitting iteratively the analytical curves given by Eqs. (3)–(6) to the experimental stress values obtained by means of PS. Table 1 gives the full set of results for the b value as obtained experimentally and as calculated according to the available analytical models. An average value of 0.273 mm for b upon applying heavy loads could be found, which is very close to the value of $t/3$ ($t = 0.820$ mm for the present sample), as proposed by Shetty et al. There are not significant differences among the b values shown in Table 1, thus confirming the approach proposed by de With and Wagemans,[3] who simply retrieved b by fitting the experimental results to Eqs. (10) and (11). In other words, an agreement could be found for the radial and tangential stresses given by Vitman and Pukh and by Kirstein and Wooley for $r = b$.

Fig. 3 shows the results of the PS analysis on the loaded sample in comparison to theoretical calculations and FEM simulation. It is clear that the approximation of "uniform constant" stress in the $0 < r < b$ region is not appropriate and can lead to an error in the order of 10% in calculating the stress magnitude at the edges of the central zone. On the other hand, PS results, theoretical and FEM computations show negligible (i.e., in the range of 1%) discrepancy outside the central area. Theoretical predictions according to Eqs. (9)–(12) fit within a degree of accuracy the experimental data (cf. Table 1).

4.2. Effect of the finite size of the fluorescence probe

Note that, given the high transparency of the polycrystalline alumina sample, the finite size of the laser probe might also affect the precision of the measurement.[13] Considering that in the focal plane the probe diameter is only about 1 μm, we shall ignore here the probe effect in the measurement plane and only assess the effect of a finite probe depth (i.e., about 30 times larger than the diameter). The intensity distribution of the fluorescence emission within the laser probe can be described by a probe response function, $B(z, z_0)$, which expresses the contribution to the entire emission intensity of the light scattered from the point $P(z)$ when the incident beam is focused at the point $P_0(z_0)$[14,15]:

$$B(z, z_0) \propto \frac{p^2}{(z - z_0)^2} e^{-2\alpha z} \tag{14}$$

where p is the probe response parameter (in polycrystalline alumina with grain size of about 1 μm, $p = 75$ μm[13]) and α is the absorption coefficient of the material at the incident wavelength. Note that the term 2α in Eq. (14) should be substituted by the sum of the absorption coefficients for incident and emitted light (i.e., $2\alpha = 0.036$ for polycrystalline alumina),[13] when the absorption conditions for incident and emitted light are different. Then, the distribution within the probe of the externally applied load introduces an hydrostatic stress state, $\overline{\sigma_h(z_0)}$, which is weight-

Table 1
Comparison between calculated (i.e., by Eqs. (9) and (12)) and experimental stress and b values at different loading levels.

Load P (N)	b Eq. (12) (mm)	b_{exp} (mm)	σ_h Eq. (9) (MPa)	$\sigma_{h\,max\,exp}$ (MPa)
52.0	0.273	0.3 ± 0.1	93	101 ± 20
105.5	0.273	0.275 ± 0.03	203	186 ± 19
150.1	0.273	0.273 ± 0.02	291	275 ± 16
200 N	0.273	0.273 ± 0.02	385	372 ± 18

averaged by the probe response function (Eq. (14)), according to the following equation:

$$\overline{\sigma_h(z_0)} = \frac{\int_0^\infty B(z, z_0)\sigma_h(z)\,dz}{\int_0^\infty B(z, z_0)\,dz} \tag{15}$$

Numerically solving the above integral by introducing as a trial function the Eq. (2) (with the stress functions according to Eqs. (3) and (4)), one can obtain the "true" stress function from its probe-averaged value at any point geometrically coincident with the center of the probe in the focal plane. Such a deconvoluted stress is also shown in Fig. 3.

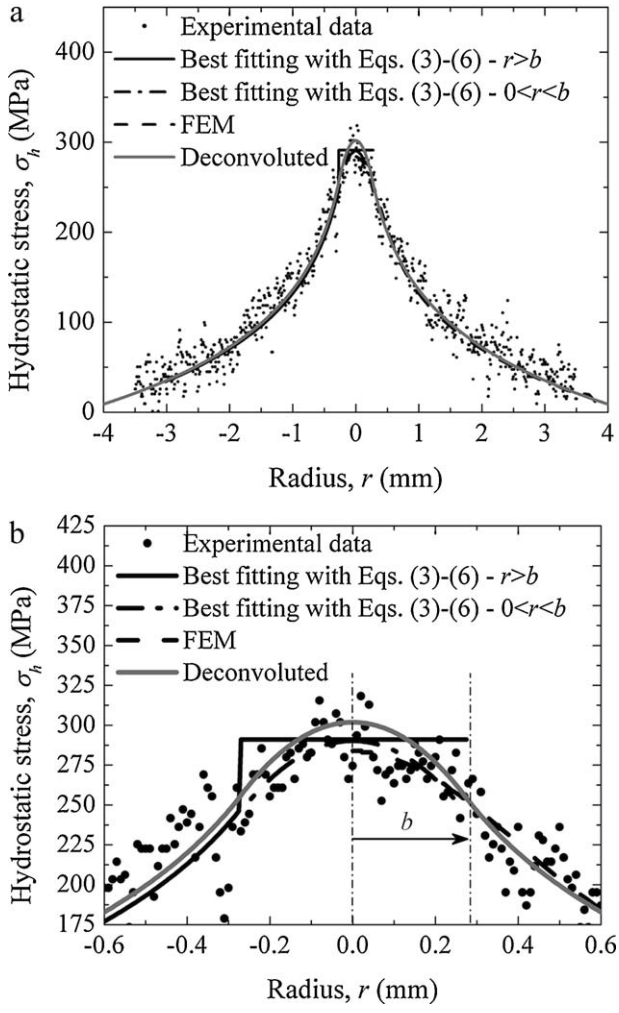

Fig. 3. (a) PS experimental stress distribution along a radial direction on the surface of a disk sample loaded by 150.1 N in the ball-on-ring jig is compared to a theoretical prediction and to FEM computations; (b) an enlarged plot of the central area of the loaded sample. A constant line shows the approximation of constant stress in the central zone of diameter $2b$. A deconvoluted stress function, which takes into account the smoothing effect by the finite laser probe depth, is also shown as computed according to Eq. (15).

The present assessment of the averaging effect by the laser probe shows that, in the present ball-on-ring configuration, the stress gradient along the in-depth axis gives an impact on stress magnitude information in the order of about 4%, thus a minor contribution as compared to the experimental scatter due to the polycrystalline nature of the solid (cf. Fig. 3). Thus, we confirmed the results obtained in the previous section, showing the validity of the Kirstein and Wooley's solution for $0 < r < b$ as compared to the "constant" stress region model.

5. Conclusion

Theoretical models for calculating the stresses developed in a polycrystalline alumina plate loaded in a ball-on-ring biaxial flexure jig have been revisited with emphasis placed to unfold the stress field at the center of the disk. Stresses were experimentally measured with high spatial resolution according to the PS method applied to the chromophoric emission from alumina and a comparison carried out with theoretical equations by various authors and with stresses simulated via finite element modeling. From the results, it appears that despite the presence of a uniform pressure within the loading region (i.e., $0 < r < b$), considering the stress distribution as a constant is incorrect. On the other hand, the Kirstein and Wooley's solution for $0 < r < b$ showed very good agreement with the stress distribution data obtained by the PS method, provided that a large enough number of supporting points are used in the computation to approximate the supporting action of a continuous ring. FEM simulation also indicated a complex stress distribution within a tiny interval surrounding the b radius value. The maximum value calculated by finite element modeling was only 1% lower than that predicted by theory and 5% lower than that measured by means of PS after spatial deconvolution of the probe. The b value experimentally retrieved with micrometric spatial resolution was in good agreement with previous assessments made by de With and Wagemans.[3]

References

1. Kirstein AF, Woolley RM. Symmetrical bending of thin circular elastic plates on equally spaced point supports. *Res Natl Bur Stand* 1967;**71**(1):1–10.
2. Shetty DK, Rosenfield AR, McGuire P, Bansal GK, Duckworth WH. Biaxial flexure tests for ceramics. *Am Ceram Soc Bull* 1980;**59**(12):1193–7.
3. de With G, Wagemans HM. Ball-on-ring test revisited. *J Am Ceram Soc* 1989;**72**(8):1538–41.

4. Hsueh CH, Lance MJ, Ferber MK. Stress distributions in thin bilayer discs subjected to ball-on-ring tests. *J Am Ceram Soc* 2005;**88**(6):1687–90.
5. Shetty DK, Rosenfield AR, Duckworth WH, Held PR. A biaxial-flexure test for evaluating ceramic strengths. *J Am Ceram Soc* 1983;**66**(1):36–42.
6. Shetty DK, Rosenfield AR, Bansal GK, Duckworth WH. Biaxial fracture studies of a glass–ceramic. *J Am Ceram Soc* 1981;**64**(1):1–4.
7. Vitman F, Pukh VP. A method for determining the strength of sheet glass. *Zavod Lab* 1963;**29**(7):863–7.
8. Westergaard HM. Stresses in concrete pavements computed by theoretical analysis. *Public Roads* 1926;**7**(2):25–35.
9. Ma Q, Clarke DR. Piezospectroscopic determination of residual stresses in polycrystalline alumina. *J Am Ceram Soc* 1994;**77**(2):298–302.
10. Wan K, Zhu W, Pezzotti G. Methods of piezo-spectroscopic calibration of thin-film materials. I. Ball-on-ring biaxial flexure. *Meas Sci Technol* 2006;**17**:1190–811.
11. Merlani E, Schmid C, Sergo V. Residual stresses in alumina/zirconia composites: effect of cooling rate and grain size. *J Am Ceram Soc* 2001;**84**(12):2962–8.
12. Pezzotti G, Müller WH. Micromechanics of fracture in a ceramic/metal composite studied by in situ fluorescence spectroscopy. II. Fracture mechanics analysis. *Continuum Mech Thermodyn* 2004;**16**(5): 471–9.
13. Pezzotti G, Munisso MC, Lessnau K, Zhu W. Quantitative assessments of residual stress fields at the surface of alumina hip joints. *J Biomed Mater Res B Appl Biomater* 2010;**95**(2):250–62.
14. Lipkin DM, Clarke DR. Sample-probe interactions: sampling microscopic property gradients. *J Appl Phys* 1995;**77**(5):1855–63.
15. Atkinson A, Jain SC. Spatially resolved stress analysis using Raman spectroscopy. *J Raman Spectrosc* 1999;**30**:885.